Photoacoustic Effect Studies Carried Out on Tissue-Mimicking Phantoms

Doku Benzeri Fantomlar Üzerinde Gerçekleştirilen Fotoakustik Etki Çalışmaları

Hüseyin Okan Durmuş

TUBITAK National Metrology Institute (TUBITAK UME), Medical Metrology Laboratory & Gebze Technical University, Physics Department, Kocaeli, Türkiye

Prof. Dr. MirHasan Yu. Seyidov

Gebze Technical University, Physics Department, Gebze-Kocaeli, Turkey

** Corresponding author: huseyinokan.durmus@tubitak.gov.tr, hokandurmus@gtu.edu.tr*

Geliş Tarihi / Received: 08.06.2022
Kabul Tarihi / Accepted: 25.07.2022
Araştırma Makalesi/Research Article
DOI: 10.5281/zenodo.6948354

ÖZET

Hem fotoakustik spektroskopi hem de fotoakustik görüntüleme çalışmaları fotoakustik etki ilkesine dayanmaktadır. Farklı yapılara sahip doku benzeri malzemelerin fotoakustik etkilerinin araştırılması bilim camiasına değerli bilgiler sağlayabilir. Bu çalışmada, içi hava ile dolu hücre tipi bir fotoakustik ölçüm sistemi geliştirilmiştir. Fotoakustik ölçüm sistemi, sürekli dalga lazer sistemi, kıyıcı/chopper, kilitli amplifikatör ve içinde hassas bir mikrofonun yer aldığı deneysel bir hücreden oluşturulmuştur. Bir kıyıcı ile birlikte çalışan sürekli dalga lazer ışığı, hücre içine yerleştirilen farklı doku benzeri malzemelere yansıtılmış ve bu şekilde farklı doku benzeri malzemelerin fotoakustik etkilerinin elektrik sinyalleri elde edilmiştir. Elektrik sinyallerinden elde edilen spektrumlar, çeşitli kıyıcı frekanslarında çıkarılmıştır. Ayrıca, bu çalışmada fantomların makroskopik ve mikroskobik optik parametrelerinin de fotoakustik ölçümlerden belirlenebileceği yenilikçi bir şekilde gösterilmiştir.

Anahtar Kelimeler: Fotoakustik Etki, Doku Benzeri Fantomlar, Agar, Zerdine, Kas Fantomu, Elektriksel Sinyaller, Fotoakustik Spektroskopi, Fotoakustik Görüntüleme

ABSTRACT

Both photoacoustic spectroscopy and photoacoustic imaging studies are based on the principle of photoacoustic effect. Investigating photoacoustic effects of tissue-mimicking materials with different structures can provide valuable information for the scientific community. In this study, a cell-type photoacoustic measurement system filled with air was developed. The photoacoustic measurement system was composed of a continuous-wave laser system, chopper, lock-in amplifier, and an experimental cell inside which a sensitive microphone was located. Continuous-wave laser light, working together with a chopper, was projected onto different tissue-like materials placed in the cell and the electrical signals of photoacoustic effects of different types of tissue-mimicking materials were obtained in this way. The spectra obtained from electrical signal were extracted at various chopper frequencies. Furthermore, it was also shown in an innovative way that the macroscopic and microscopic optical parameters of phantoms can be determined from photoacoustic measurements.

Keywords: Photoacoustic Effect, Tissue-Mimicking Phantoms, Agar, Zerdine, Muscle Phantom, Electrical Signals, Photoacoustic Spectroscopy, Photoacoustic Imaging

1. INTRODUCTION

Photoacoustic (PA) or Optoacoustic (OA) effect is the production of acoustic waves formed by the absorption of modulated electromagnetic waves by the material (Musdal & Kurt, 2021). Photoacoustics is a hybrid technique that combines optics and acoustics (Chen, Qin, Qi, & Xi, 2021). The photoacoustic technique is a variation of the photothermal effect, which is based on the light

striking the sample and altering the thermal state of the sample. In other words, the photoacoustic effect is a conversion between light, heat, and sound as a result of light absorption. It is an opto-thermo-acoustic conversion that occurs on a material (Tan, 2018).

Alexander Graham Bell, the inventor of the telephone, discovered the Photoacoustic effect in 1880. Graham Bell utilized his "spectrophone" to listen to the sound generated by materials that absorb sunlight at different wavelengths. Bell discovered that sound propagates when light is focused on a thin diaphragm (Liu L. , ve diğerleri, 2021) (Hosseinaee, Le, Bell, & Reza, 2020) (Liu L. , ve diğerleri, 2021) (Thakur, 2018). Photoacoustic (PA) and photothermal (PT) phenomena begin with Graham Bell's photophone (Musdal & Kurt, 2021).

The photoacoustic technique, which was originally utilized solely for the examination of gas samples, has been successfully expanded to the analysis of condensed matter after the successful development of a general theoretical model (Tan, 2018).

The application of the photoacoustic effect to solids was first modeled in a gas microphone system by Rosencwaig and Gersho in 1976. The signal, simplified in one dimension, was interpreted through the link between the heat conduction and pressure wave generation in a hermetically sealed PA cell (Liu L. , ve diğerleri, 2021).

In his investigations, Bell discovered that pulsed intense light could heat optically absorbent materials, causing them to expand and produce audible vibrations. Bell demonstrated that dark fibers generate louder noise than lighter fibers; this is also compatible with the current photoacoustic relationship, which states that the amplitude of the photoacoustic signal produced is proportional to the quantity of light absorbed. Bell used a prism to split white light, demonstrating that different color combinations of light and fibers may generate louder sounds. Multi-wavelength photoacoustic imaging, which changes the wavelength of light and relates the amplitude of the photoacoustic response to the absorption spectra of the materials being imaged, employs the same idea today. The creation of medical images of biological chromophores typically present in tissues, which absorb light energy and cause photoacoustic transitions, is a contemporary use of the photoacoustic phenomenon. Ultrasonic transducers on the outer surface of the tissue can absorb photoacoustic pressure waves, making photoacoustic imaging a non-invasive, non-ionizing medical imaging method with ultrasound-like resolution at considerable tissue depth. Photoacoustic imaging is a new biomedical imaging technique that uses acoustic detectors to view optical absorbers within tissues (light input–sound output) (Bayer, Luke, & Emelianov, 2012).

Currently, FTIR (Fourier transform infrared spectrophotometry) devices employ photoacoustic spectroscopy. However, it has been implemented in FTIR only in the last two decades. The sample was placed in a container and covered with an IR-transparent glass in a photoacoustic accessory. Subsequently, the accessory was filled with either helium or air. The IR beam was then directed onto the sample. Helium absorbed heat from the sample and expanded, causing the pressure to increase and flow to form. The movement of helium within the sample cell produces sounds, which are translated into electrical signals using a microphone. An interferogram was created by plotting the microphone signal against the path difference. A carbon black spectrum was employed as a background. To obtain the spectra, Fourier transform was used to convert the interferogram. Solids, liquids, and gases can be studied using photoacoustic spectroscopy (PAS). It is a nondestructive method that does not require significant sample preparation (Subramanian, 2009).

The value of PAS was first understood in the 1970s, when tunable lasers became available. Progress in electronic instrumentation, easy access to computers, and the availability of tiny acoustic detectors have considerably increased the scope of PAS in laboratory and distant sensing applications over the last four decades (Thakur, 2018).

Several alternative detection methods for receiving photoacoustic waves have been used over the years, including quartz tuning forks, membrane microphones in resonant cells, and cantilever and bridge acoustic sensors for miniature detectors. Special sensor designs, such as those utilizing optical

resonance cavities to increase light-gas interactions, have been proposed to improve performance (Photoacoustic spectroscopy for gas sensing: from theoretical modeling to applications, 2022).

In the 1970s and the 1980s, a variety of industrial and scientific sensing applications were developed. However, indirect gas-phase cell-type PA detection has been used in many of these applications, where acoustic waves propagating in a gas generated by laser-induced surface heating are detected using a microphone. This is in contrast to biological PA imaging (PAI), which benefits from the direct detection of laser-induced ultrasonic waves (Beard, 2011).

Although Alexander Graham Bell initially characterized the photoacoustic effect as the conversion of optical energy into sound pressure waves over a century ago, research on the photoacoustic effect made little progress until the invention of the laser allowed for much more advanced signal generation. Photoacoustics became more popular afterwards, first in the field of gas spectroscopy and then in biomedical applications. PAI has progressed rapidly from idea to tomographic modality for small-animal imaging to clinical devices in the last 20 years (Steinberg et.al, 2019).

When an atom receives sufficient energy from the outside, an electron in one of its orbitals travels from that energy level to another orbital with a higher energy level. This phenomenon is known as the excitation of an atom. These atoms are called the excited atoms. An excited electron always tends to return to its ground state, and while doing so, releases energy in the form of light at a certain frequency. In other words, the received energy is emitted as energy again, but in photoacoustic effect case, it changes from light to heat energy as it moves along. A sound wave can be created in the audible area of the audio spectrum if the relaxation period of these molecules is less than the duty cycle of the optical signal (Musdal & Kurt, 2021).

A periodically modulated laser beam is directed onto the material. Some or all of the absorbed light energy is converted into heat through nonradiative excitation processes. Consequently, there was a constant heat supply. If a solid sample is enclosed in a gas-tight cell, alternative expansion and contraction of the gas layer adjacent to the solid surface is induced owing to the modulated surface temperature. Depending on the properties of the sample, a photoacoustic pressure signal is generated (Herrmann, Pech-May, & Retsch, 2021). The acoustic transitions that appear are wideband and detectable using an ultrasonic transducer (Su, ve diğerleri, 2010).

Measurement of photoacoustic spectroscopy measurements are based on the photoacoustic effect. When a material is exposed to pulsed light, it generates acoustic waves with the same frequency as that of the light. Several decades have passed since the photoacoustic effect was later applied as a measurement technique. With the advent of highly sensitive microphones and other advancements in electronics, studies have shifted to measuring gas samples in particular. This is a novel approach for using the photoacoustic effect in the infrared range. This method has been intensively studied for solid sample examination owing to the advent of highly sensitive FTIR equipment (Sawada, 1982).

Photoacoustic spectroscopy is one of the most powerful techniques for gas detection, covering a wide range of applications, including atmospheric monitoring, industrial process control, safety, and biomedical applications (Photoacoustic spectroscopy for gas sensing: from theoretical modeling to applications, 2022).

Photoacoustic (PA) spectroscopy, also known as opto-acoustic spectroscopy, is part of a family of optothermal (OT) techniques based on converting optics to thermal energy. Different approaches for the examination of solid, liquid, and gaseous samples have been developed over the last century, depending on how this thermal energy is created and detected (Haisch, 2011). PA spectroscopy can be divided into three categories: gas and aerosol measurements, liquid and soft material applications, and solid measurements (Haisch, 2011).

Photoacoustic techniques have several advantages. It can be applied to a wide variety of samples such as solids, liquids, and gases (Haisch, 2011). This offers the possibility of a nondestructive analysis (Subramanian, 2009). It is highly safe because it does not contain ionizing radiation (Steinberg et.al., 2019). It is unaffected by the phenomenon of “optical scattering” in optical imaging modalities

(Oraevsky, ve diğerleri, 2018). Photoacoustic imaging (PAI) is an advanced imaging modality compared to optical imaging and ultrasonic imaging techniques because it is a hybrid imaging modality that combines the benefits of optical and ultrasonic imaging (Zhou & Jokerst, 2020). It provides non-invasive imaging (Zhang, Hong, & Cai, 2011). It allows for in vitro and in vivo analyses and imaging (Tan, 2018). The structural, functional, and molecular imaging of living organisms can be performed (Zhang, Hong, & Cai, 2011). It can detect diseased tissues or processes such as cancer (Su, ve diğerleri, 2010). The depth profile provides information about deeper tissue penetration or deeper imaging depth (Chen, Qin, Qi, & Xi, 2021). It offers better absorption by contrast agents (Zhang, Hong, & Cai, 2011). It has the ability to display both endogenous (with oxyhemoglobin (HbO2), deoxyhemoglobin (Hb), water (both free and bound), melanin, and lipid)) and exogenous (small molecule dyes such as methylene blue dye (MBD), indocyanine green (ICG), reporter gene agents, and nanoparticles) chromophores (Steinberg, ve diğerleri, 2019). It has high spatial and temporal resolution potential (Steinberg, ve diğerleri, 2019). It offers a higher spatial resolution with the possibility of high ultrasonic resolution (currently, the spatial resolution is approximately 100 μm) (Zhang, Hong, & Cai, 2011) (Mehra, Jain, & Jain, 2016). It has good image contrast (excellent soft-tissue contrast) (Zhang, Hong, & Cai, 2011) (Manohar & Gambhir, 2020). It has high specificity and sensitivity (which are affected by the sample size. The sensitivity decreases with an increase in the sample size. It has a high sensitivity to blood volume and blood oxygen saturation.) (Tan, 2018) (Subramanian, 2009) (Manohar & Gambhir, 2020). For now, it can use Optical and RF electromagnetic waves (Tan, 2018) (Zhang, Hong, & Cai, 2011). It offers the possibility of producing a relatively inexpensive biomedical imaging device (handheld photoacoustic probe) (Hariri, ve diğerleri, 2018). This may pave the way for many applications in physics, materials science, and medicine, with its finding a wider application area in the future (Tan, 2018).

There are two main applications for photoacoustic effect. One is photoacoustic spectroscopy, and the other is photoacoustic imaging. As another classification, a distinction can be made between biological and non-biological photoacoustic applications. Photothermal spectroscopy (PTS) and PAS were used to examine the density changes and pressure waves generated in the gas sample owing to light absorption. Photothermal and photoacoustic effects result from the absorption of modulated light in a gas sample (Pinto, ve diğerleri, 2021). Using photoacoustic effect, light absorption in gases (Photoacoustic Spectrometer) (Tan, 2018), measurement of gaseous samples (Photoacoustic spectroscopy for gas sensing: from theoretical modeling to applications, 2022) or solid materials (Krishnaswamy, 2008), analysis (Tan, 2018) (Subramanian, 2009) (Beard, 2011) (PhotoAcoustic Imaging (PAI), 2022), investigation of the properties and behavior of materials (Tan, 2018), detection of methane gas in nitrogen (Tan, 2018), detection of ethylene, ammonia and other gases in the air (Tan, 2018), environmental monitoring of chlorofluorocarbons (CFC) compounds in the atmosphere, greenhouse gases (GHG) and carbon monoxide, as well as hydrocarbon leakage detection in pipeline transport systems (Pinto, ve diğerleri, 2021), ozone gas detection applications such as monitoring (Keeratirawee & Hauser, 2021), and soil analysis (Volkov, Rogova, & Proskurnin, 2020) can be given as examples of non-biological photoacoustic applications.

The other main application based on the photoacoustic effect is photoacoustic imaging. This imaging technique is also known as optoacoustic (OA) or thermoacoustic (TA) imaging. While photoacoustic imaging uses pulsed light to excite the sample, the term "thermoacoustic imaging" refers to the utilization of electromagnetic radiation in the radio frequency and microwave ranges (Tan, 2018). Photoacoustic effect is a more general term where the waves produced have any detectable frequency, while the photothermal effect is a more common term in laser surgery and ablation. Medical imaging is important in the field of medicine for the diagnosis and treatment of diseases. Therefore, it is important to use effective imaging systems to examine the internal structure of organs in detail and to provide early diagnosis and treatment of diseases. In the last century, many researchers have used light sources to optically visualize cellular and molecular functions in the body, such as X-ray radiography, computed tomography (CT), elastography, ultrasonography (USG), magnetic resonance imaging (MRI), radionuclide imaging, positron emission tomography (PET), and single-photon

emission computed tomography (SPECT). However, in addition to these imaging techniques, many other imaging techniques are also being investigated. One of the most ambitious medical imaging techniques in recent years is photoacoustic imaging. Photoacoustic imaging studies are currently considered the most innovative imaging modality in the medical field, and research on this subject is increasing every year around the world. In short, photoacoustic imaging is based on the principle of photoacoustic effect.

Ultrasound transducers on the outer surface of the tissue can detect photoacoustic pressure waves, making photoacoustic imaging a non-invasive, non-ionizing medical imaging modality similar to ultrasound with significant tissue depth resolution. The concept of photoacoustic imaging was initially presented in the mid-1990s, and the first reports of the use of the photoacoustic effect for imaging live animals appeared nine years later. There are several in vivo demonstrations of photoacoustic imaging with biological applications in medical diagnostics. The growth of medical applications in clinical photoacoustic imaging has been fueled by the study of brain vasculature and its function, as well as cancer, cardiovascular, and tissue engineering scaffolds. Most imaging techniques create contrast between anatomical characteristics inside tissue; for instance, in an ultrasound image, the difference in acoustic impedance between soft tissue and the tumor creates contrast. A nanosecond pulsed laser is utilized in modern photoacoustic imaging systems to create transient pressure waves, which are received and processed by an ultrasonic transducer (Bayer, Luke, & Emelianov, 2012). Photoacoustic imaging is an imaging method that derives image contrast from the optical absorption coefficient of the imaged tissue (Zhang, Hong, & Cai, 2011) because optical absorption can reveal various physiological parameters such as hemoglobin/melanin/water/ion concentration and oxygen saturation in living subjects. Photoacoustic signals generated by energy-absorption events caused by pulsed laser light are utilized for imaging (Su, ve diğerleri, 2010). With deeper penetration or greater resolution than other functional imaging modalities, the photoacoustic imaging method can discriminate between healthy and diseased tissues (Su, ve diğerleri, 2010). Photoacoustic imaging systems can be split into two types: Photoacoustic tomography (PAT) and Photoacoustic microscopy (PAM), which are promising structural, functional, and molecular imaging techniques for a wide range of biological applications (Zhang, Hong, & Cai, 2011). Molecular photoacoustic (MPA) imaging has recently attracted considerable interest (Steinberg, ve diğerleri, 2019).

Photoacoustic imaging can also be applied to biological and non-biological samples. The application of photoacoustic spectroscopy and tomography to living specimens (Oraevsky, ve diğerleri, 2018), full three-dimensional (3D) thermoacoustic imaging of biological tissues (Tan, 2018), in vivo tumor and angiogenesis imaging (Tan, 2018), blood oxygenation mapping (estimation of blood oxygen saturation, demonstration of oxygenation status) (Manohar & Gambhir, 2020), mapping functional cerebral hemodynamic changes in blood vessels (creation of excellent images of blood vessels) (Tan, 2018), functional neuroimaging (brain) imaging (the structure and function of rat brains in vivo using noninvasive transdermal and transcranial imaging) (Park, ve diğerleri, 2020), two functional parameters in in vivo rat brain simultaneous transcranial imaging of hemoglobin oxygen saturation (sO2) and total hemoglobin concentration (HbT) (Tan, 2018), and imaging of brain, breast cancer, psoriasis, and skin lesions (Manohar & Gambhir, 2020), with a higher resolution of deeply embedded tumor cells to the tissue, blood vessels, and lymph nodes imaging (Tan, 2018), detection of inflammation in humans (diagnosis and monitoring of inflammation) (Manohar & Gambhir, 2020), detection of skin melanoma (imaging of melanoma (skin cancer) on the skin surface and revealing the structural connection between nearby tissues such as melanoma and blood vessels in vivo) (Tan, 2018), and non-invasive 2D images of blood vessels in vivo (Tan, 2018) are some applications of photoacoustic imaging in biological samples. Photoacoustic imaging will likely remain a very vivid area of research in the coming years.

Photoacoustic techniques have also been applied to liquid samples. In their paper "Blood glucose measurements with photoacoustics," Ashton et al. (Ashton, ve diğerleri, 1999) used the near-infrared pulsed photoacoustic technique for glucose concentration measurement and demonstrated that the

measured photoacoustic signal was proportional to the glucose concentration in both in vitro and in vivo experiments, and the values found were consistent with the results obtained by the standard clinical method. In Tabaru and Saraçoğlu's (Tabaru & Saraçoğlu, 2014) paper titled "Glucose Detection with Pulsed Laser Diode Stimulated Photoacoustic Method," the signal outputs proportional to the glucose concentrations of the determined samples were obtained using the Photoacoustic (PA) method. Each sample was excited with laser pulses to prepare gel samples with different glucose concentrations. The acoustic wave generated by the laser pulses was detected by the piezo film transducer and as a result of the experiment, it was found that the amplitudes of the acoustic responses received changed linearly with the glucose concentrations of the samples.

Tissue-mimicking materials (TMMs), often known as phantoms, are widely used in medical imaging research, machine calibration and characterization, performance testing of medical systems, development of new transducers, systems or diagnostic techniques, training, surgical planning, and clinical simulators to mimic the characteristics of real human tissues. TMMs are used in medical research as idealized tissue models to create and evaluate procedures, systems, and clinical instruments. Phantoms have been used as test models for many years in both imaging and therapeutic applications. In addition, biopolymers (gellan gum, gelatin, agar, and agarose) and chemically produced polymers (polyvinyl chlorides, polymerized siloxanes, polyvinyl alcohol, etc.) are used to produce TMMs and phantoms (Rajeshkumar, Vishnupriyan, & Selvadeepak, 2020) (McGarry, ve diğerleri, 2020) (Thouvenot, Poepping, Peters, & Chen, 2016) (Culjat, Goldenberg, Tewari, & Singh, 2010). The tissue-mimicking materials used in this study were chosen as test specimens because they are suitable materials for soft and muscle tissues.

In this research, we aim to obtain electrical signals of photoacoustic effects by dropping pulsed laser light on different tissue-mimicking materials by forming a photoacoustic measurement system consisting of a continuous-wave laser system, chopper, lock-in amplifier, and sensitive microphone within an experimental cell. In other words, our main goal is to prove the photoacoustic effect on tissue-like materials and then to extract optical parameters from the obtained electrical signals. Some deductions for material analysis/characterization, photoacoustic spectroscopy, and photoacoustic imaging were made from the acquired electrical signals. It was also demonstrated that photoacoustic measurements may be used to estimate the macroscopic (such as absorbance, transmittance, reflection, refractive index, and attenuation coefficient) and microscopic (such as absorption coefficient, scattering coefficient, and reduced scattering coefficient using the Kubelka-Munk function method) optical properties of phantoms.

2. THEORY

2.1 Photoacoustic Effect Pressure Wave Equation

A brief explanation of the main equation for the pressure responsible for initiating a photoacoustic wave is as follows: Light pulses are sent to the biological tissue, which then absorbs the light and converts it to heat, after which an initial pressure increase occurs owing to thermoelastic expansion. The initial pressure leads to a photoacoustic signal, which is then detected by a transducer. The equation for the process is as follows:

$$\left[\nabla^2 - \frac{1}{c_s^2}\frac{\partial^2}{\partial t^2}\right] p(\vec{r}, t) = -\frac{\beta}{C_p}\frac{\partial H(\vec{r},t)}{\partial t} \qquad (1)$$

where cs is the speed of sound; β is the thermal expansion coefficient; Cp is the specific heat; H is the energy per unit volume and time deposited by the optical radiation beam; and p(r→,t) is the pressure of the acoustic wave, which is a function of space and time.

The heating function H is assumed to be the result of a chromophore absorber with an optical absorption coefficient μa and is heated by an optical pulse with this fluency F (energy per unit area). H was assumed to be a separable function of space and time. Thus, the heating equation is $H(r\rightarrow,t)=\mu_a F A(r\rightarrow)I(t)$. Here, $A(r\rightarrow)$ is a function of space that defines the geometry of the absorber. Similarly, I(t) describes the time dependence of the incoming optical pulse (Baddour & Mandelis, 2015).

Based on this equation, photoacoustic pressure propagation was driven by the first-time derivative of the heating function. Therefore, time-invariant heating did not generate photoacoustic pressure waves. In other words, for the photoacoustic effect to occur, a light pulse falling on a sample must meet the thermal and stress limiting conditions; otherwise, no signal will be produced. The sample should also contain absorbing chromophores at the measurement wavelength (Beard, 2011).

When both the thermal and stress confinements are met, thermal expansion causes a pressure rise (p_0), which can be estimated by

$$p_0 = \Gamma . \mu_a . F \qquad (2)$$

where p_0 is the initial pressure rise, μ_a is the absorption coefficient (cm^{-1}), $\Gamma=\beta v_s^2/C_p$ is the Grüneisen coefficient representing the thermal and mechanical properties of the tissue, and F is the fluence of the irradiated energy (J/cm^2) (Hosseinaee, Le, Bell, & Reza, 2020).

2.2 Photoacoustic Imaging

Photoacoustic imaging uses pulsed energy irradiated into the tissue. The energy absorbed by the tissue is converted into heat, upon which rapid thermal expansion occurs, resulting in the emission of an acoustic pressure wave proportional to the flux of the irradiated energy Φ, the absorption coefficient of the irradiated medium μa, and the Grüneisen tissue coefficient Γ. This relationship is explained in Equation 1, where μa depends on the wavelength of the light and fluency depends on the wavelength of the light and the depth at which the photons are emitted. The resulting acoustic transitions were broadband and could be detected using an ultrasonic transducer. Reconstruction of the resulting image is accomplished by inverse calculation of the photoacoustic signal source, both temporally and spatially. Depending on the scanning parameters used in data collection, two-dimensional images or 3D tomographic images can be created (Su, ve diğerleri, 2010).

$$PA(\lambda, z) = \mu_a(\lambda) \cdot \Phi(\lambda, z) \cdot \Gamma \qquad (3)$$

3. METHODOLOGY

3.1 Preparation of Phantoms

Phantoms are imaging test samples with known geometric and material composition that are commonly utilized in the creation and assessment of imaging systems or algorithms in medical imaging (Cook, Bouchard, & Emelianov, 2011). The agar phantom was prepared by forming a solution of 0.4 M ZnCl2 and 2% by weight agar (Karaböce, Çetin, Durmuş, & Özdingiş, 2016). The Zerdine® phantom was produced using the formulation in Zerhouni and Rachedine's patent (Zerhouni & Rachedine, 1993). The muscle phantom was formed using a method identical to that described by Gutierrez et al. (Gutierrez, Lopez-Haro, Vera, & Leija, 2016). All phantoms were produced by cutting the main phantoms into a square shape, measuring approximately 35 mm × 35 mm × 15 mm. The calculated densities (mass/volume) of the phantoms were was found as (1.06 ± 0.03) g/cm^3 for agar

phantom, (0.98 ± 0.05) g/cm^3 for Zerdine phantom, and (1.07 ± 0,05) g/cm^3 for muscle phantom respectively.

3.2 Photoacoustic Measurement Setup and Acquisition of Photoacoustic Data

Photoacoustic measurement system consisted of a lock-in amplifier (Stanford Research Systems, SR510), a chopper controller (Stanford Research Systems, Model SR540) and its blade (inner blade 5 eye, outer blade 6 eye), an electret microphone (Maxim Integrated, MAX9814 electret microphone with amplifier modul and with 5V, 2A Raspery Pi compatible tablet adapter), a photoacoustic cell (3D Printed in our laboratory, dimensions are 5 mm width x 45 mm length x 60 mm depth, wall thickness 2.5 mm), a test material inside photoacoustic cell and a continuous-wave laser (Optotronics brand VA-I-400-635 model, 635 nm Red Color Solid-State Diode Laser). Figure 1 shows the photoacoustic experiment.

The 635 nm red continuous-wave laser beam was placed in a way that faced the sample inside the photoacoustic cell. The pulsed laser light was generated with an optical chopper placed in front of the continuous-wave laser. In this study, a pulsed laser beam was not obtained by adjusting the laser modulation frequency. A chopper was placed between the photoacoustic cell and the laser to send the pulsed light. The chopper frequency was adjusted using a chopper controller. The chooper controller was connected to the lock-in amplifier with a BNC cable. The photoacoustic cell was closed on five sides, and the surface on which the laser light fell was a closed chamber with a stretch film and air inside. The electret microphone, which had an electronic module behind it, was placed within the photoacoustic cell. An electret microphone with an electronic module was connected to a lock-in amplifier using a BNC cable. It must also be noted that the correct working frequency is the chopper frequency.

When the laser is turned on, the pulsed laser beam falls on the sample in the photoacoustic cell by the chopper, and after a certain period of time, the laser beam creates an acoustic wave, and these acoustic waves are detected by the electret microphone and transmitted the electrical signal to the Lock-In Amplifier. Simultaneously, the scanning frequency information was transmitted to the lock-in amplifier by the chopper controller. The lock-in amplifier filtered the signal from the microphone at the chopper frequency. In this way, the photoacoustic effect spectra of the material placed in the photoacoustic cell are extracted based on the chopper frequency by scanning at different chopper frequencies. If the chopper frequency is kept constant and different colored cut-off filters are used under white light, the photoacoustic spectrum of the material can be obtained. This is known as photoacoustic spectroscopy.

In all the measurement processes in this work, after the chopper frequency was adjusted, it was waited for 10 s. Then, after the lock-in amplifier voltage value was fixed, at least 10 data points were taken manually at each frequency consecutively, and this measurement process was repeated at least five times for each phantom

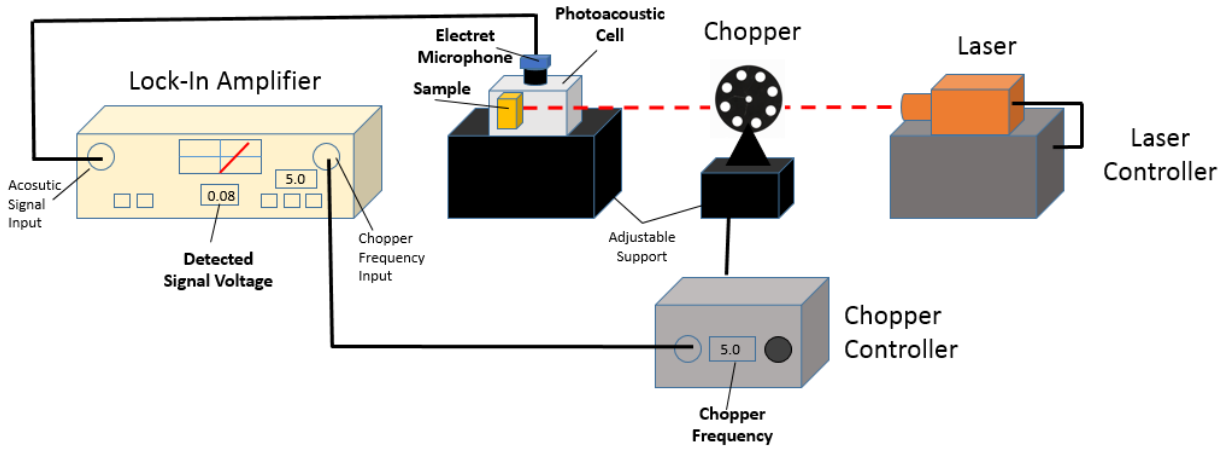

Figure 1. A picture of photoacoustic measurement setup

3.3 Calculation Formulas for Macroscopic and Microscopic Optical Parameters

The macroscopic optical parameters for absorbance, transmittance, reflectance, refractive index, and optical linear attenuation coefficient were calculated using the following formulas after I and I_o measurement (Nadeem & & Ahmed, 2000) (Harvey, 2003) (Chang & Bowden, 2019).

$$R+T+A=1 \text{ or } \%R+\%T+\%A=\%100 \quad (4)$$

$$\text{Absorbance, A; } A=-\log(I/I_0)=-\log(T)=2-\log(\%T) \quad (5)$$

$$\text{Transmittance, T; } T=I/I_0 \quad (6)$$

$$\text{Reflectance, R; } R=1-(A+T) \quad (7)$$

$$\text{Reflectance, } R=\frac{(n-1)^2}{(n+1)^2}, \quad (8)$$

where n is the Refractive Index.

$$I=I_0e^{-\mu x},\ \mu=-\frac{\ln\frac{I}{I_0}}{x} \quad (9)$$

where μ is the Linear Total Attenuation Coefficient.

The related microscopic formulas used in the calculations of the absorption coefficient, scattering coefficient, reduced scattering coefficient, and total attenuation coefficient are as follows:

The Kubelka-Munk Function is given by (Torrent & Barrón, 2008)

$$F(R)=\frac{(1-R)^2}{2R}=\frac{k}{s} \quad (10)$$

where R = Reflectance, k= Absorption Coefficient, s=Scattering Coefficient.

The total attenuation coefficient is described by (Wilson, 1995)

$$\mu = \mu_t = \mu_a + \mu_s \qquad (11)$$

Where μ_a is Absorption Coefficient and μ_s is Scattering Coefficient.

That is, k=μ_a and s=μ_s can be matched using Equations (10) and (11).

The reduced scattering coefficient (μ_s') is defined by the following equation (Jeong, ve diğerleri, 2017);

$$\mu_s' = (1 - g)\mu_s \qquad (12)$$

where, g is the anisotropy factor. The g value of the phantom was fixed at 0.98, which is the anisotropy factor of the human tissue in the UV and near-infrared spectra.

4. MEASUREMENT RESULTS AND DISCUSSION

In this study, the photoacoustic effect spectra of three different phantoms at different chopper operating frequencies and the macroscopic and microscopic optical properties of the phantoms were investigated using a constituted photoacoustic measurement system. We can determine the macroscopic and microscopic optical parameters of the phantom in photoacoustic measurements by evaluating the situations when the phantom is in the system and when there is no phantom in the system. All experiments were performed under controlled ambient laboratory conditions [temperature 23.5 °C ± 0.2 °C and relative humidity 46%rh ± 4%rh].

4.1 Measurement Results of Photoacoustic Effect Spectra of Different Phantoms

The photoacoustic spectrum of agar, Zerdine, and muscle phantoms can be seen in Figures 2 to 4, respectively. These graphs were obtained under pulsed laser light applied at different chopper frequencies, while the phantoms were inside a normal air-filled photoacoustic cell in this measurement.

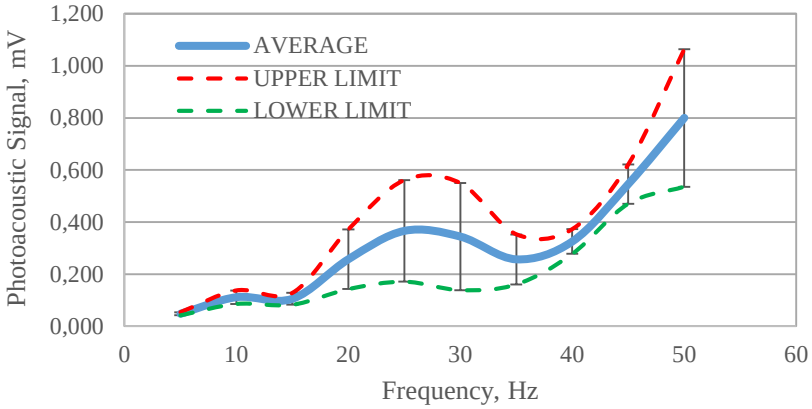

Figure 2. The obtanied photoacoustic spectrum of agar phantom at different chopper frequencies

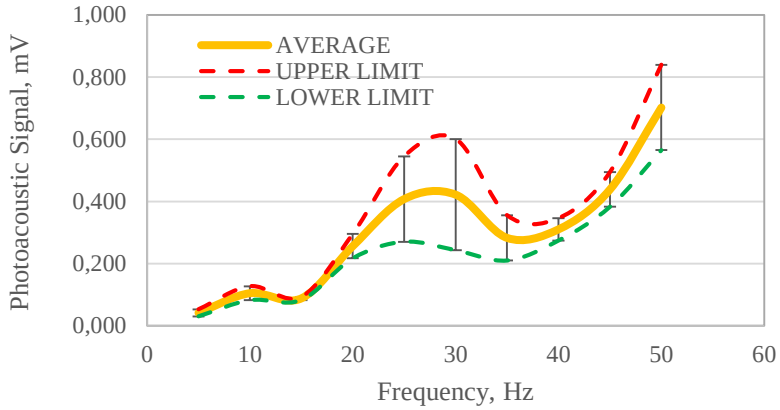

Figure 3. The obtanied photoacoustic spectrum of Zerdine phantom at different chopper frequencies

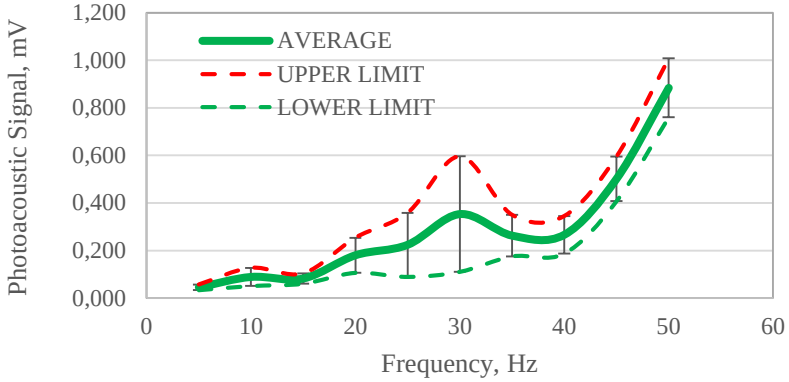

Figure 4. The obtanied photoacoustic spectrum of muscle phantom at different chopper frequencies

In Figure 5, photoacoustic spectra obtained from phantoms at different chopper frequencies are shown in a single graph. As can be seen from the figure, the constituted photoacoustic measurement system gives different spectra in phantoms with different properties. When the spectra are examined, it is seen that the agar and Zerdine phantoms show a similar tendency because they represent soft tissues. The muscle phantom, on the other hand, represents a slightly different character. This situation can be explained as follows. This is an expected situation because all three phantoms are water-based

phantoms and have the same absorber component, such as water, at an incident light wavelength of 635 nm. In addition, it can be seen that the signal powers was high in the 20-35 Hz range for each phantom. This may depend on the chemical and physical composition of the phantoms.

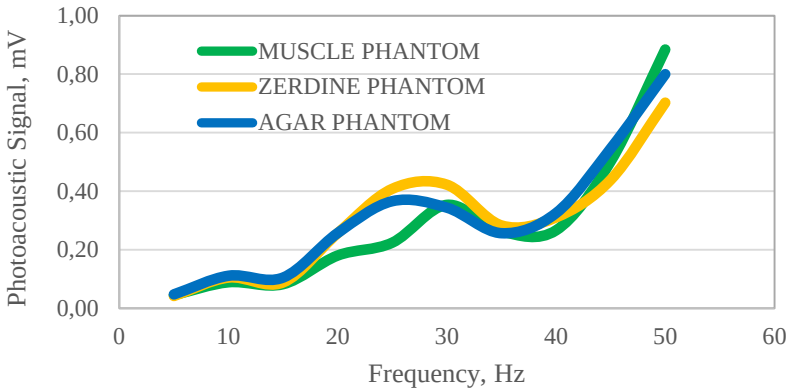

Figure 5. The photoacoustic spectrum of all phantoms at different chopper frequencies

The photoacoustic spectrum of the photoacoustic cell, which was used to denote the absence of the phantom in the measurement system, was also obtained at different chopper frequencies without placing any phantom inside the photoacoustic cell, as shown in Figure 6. Here, the pulsed light hits the cell wall of the measuring system made of ABS material instead of the phantom sample.

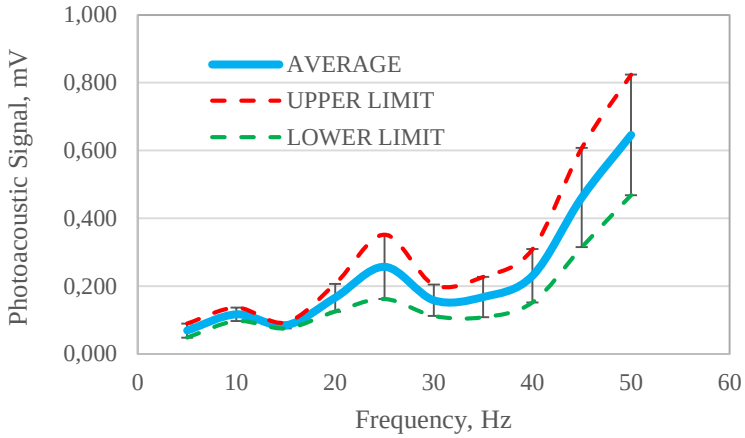

Figure 6. The photoacoustic spectrum of the photoacoustic cell without phantom at different chopper frequencies

After obtaining the photoacoustic spectrum for the photoacoustic cell system, the spectrum of the photoacoustic cell system was subtracted from the spectrum acquired for each phantom, and net photoacoustic spectra were obtained for each phantom, as shown in Figure 7, 8, and 9.

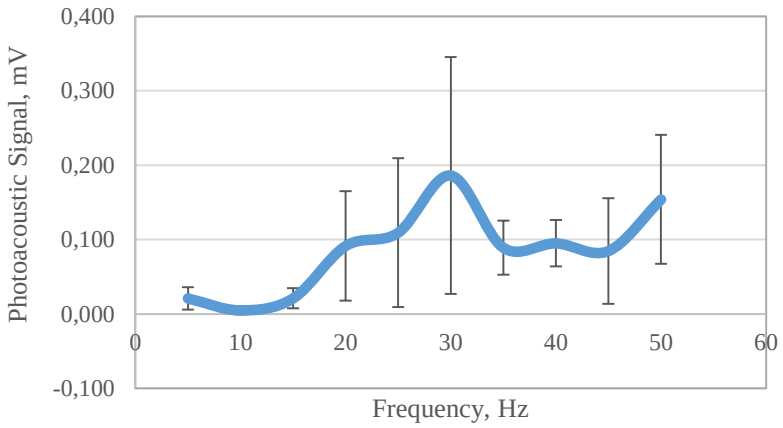

Figure 7. The photoacoustic spectrum of the net agar phantom at different chopper frequencies

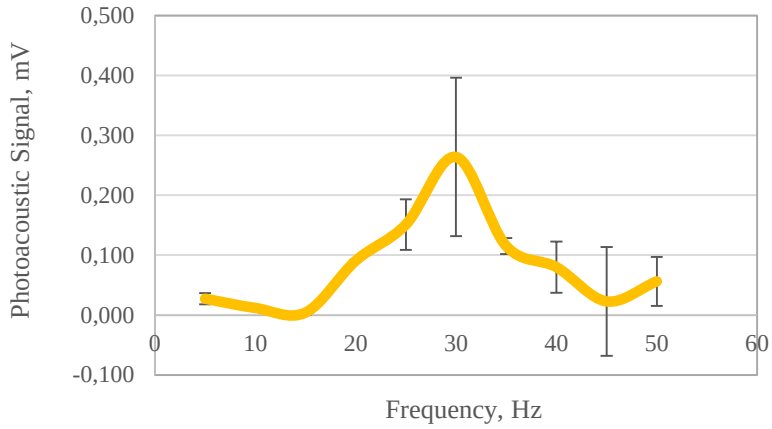

Figure 8. The photoacoustic spectrum of the net Zerdine phantom at different chopper frequencies

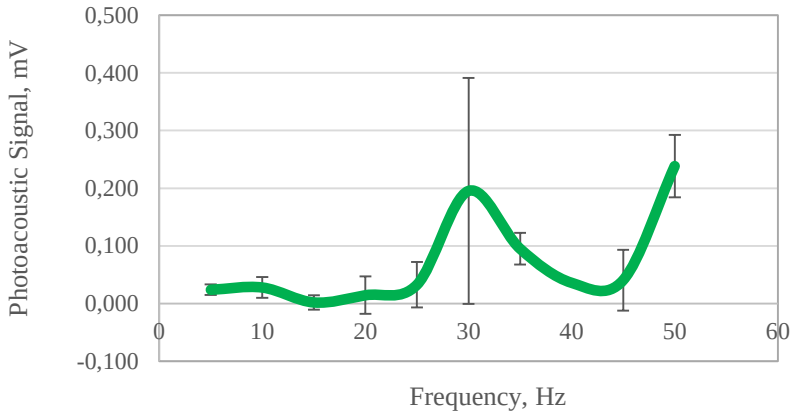

Figure 9. The photoacoustic spectrum of the net muscle phantom at different chopper frequencies

In Figure 10, the net photoacoustic spectra obtained from phantoms at different chopper frequencies are shown in a single graph. As can be seen from the figure, the spectra are more clearly separated from each other because they are phantoms with different structures, contents, and characters.

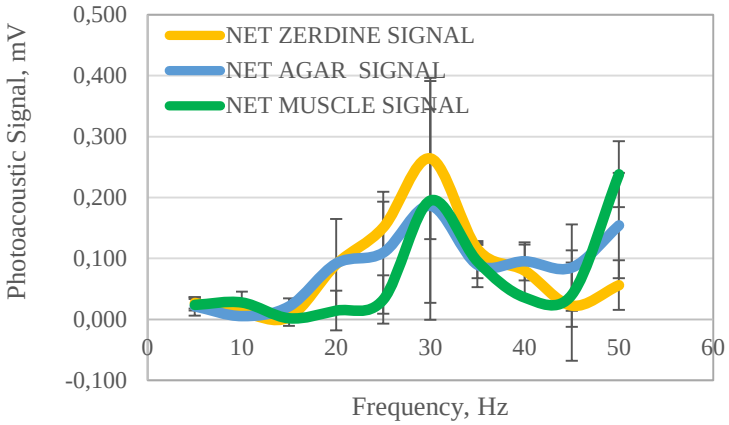

Figure 10. The photoacoustic spectrum of the net phantom signals at different chopper frequencies

We can also determine the macroscopic and microscopic optical parameters of phantoms from photoacoustic measurements by evaluating the situations when the phantom is in the system and when there is no phantom in the system at a specific chopper frequency. Here, when there is no phantom in the system, that is, the photoacoustic spectrum of the system can be evaluated as "I_o", and the photoacoustic spectrum taken when there is a phantom in the system can be evaluated as "I" and so the macroscopic and microscopic optical parameters can be calculated. In the meantime, it is important to note that the macroscopic and microscopic optical parameters of the phantoms we obtained belong to the 635 nm wavelength because we used a 635 nm continuous-wave laser light.

4.2 Measurement Results of Macroscopic Optical Parameters of Phantoms

The acquired macroscopic optical characteristics of the phantoms, such as transmittance, absorbance, reflectance, refractive index, and optical linear attenuation coefficient at 635 nm wavelength using photoacoustic measurements at a chopper frequency of 10 Hz, can be seen in Figures 11–15.

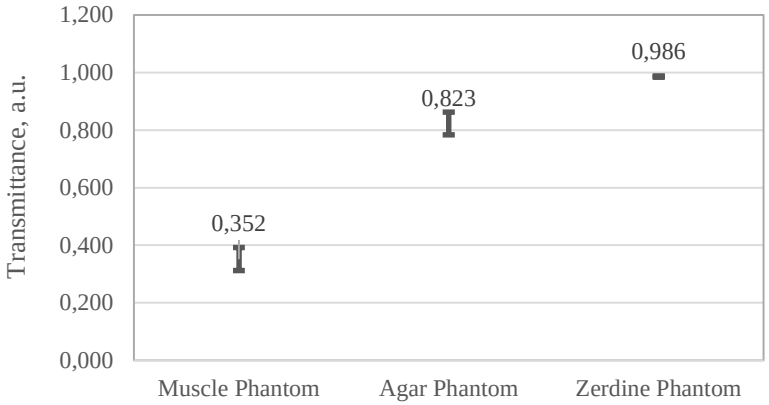

Figure 11. The trasmittance values of phantoms at 10 Hz chopper frequency for 635 nm wavelenght

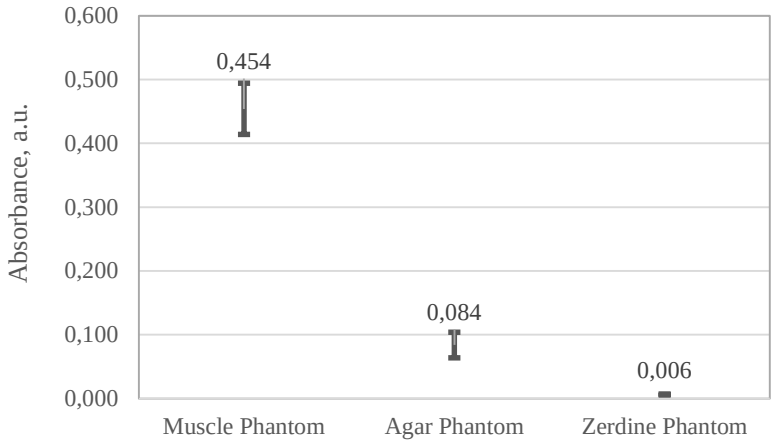

Figure 12. The absorbance values of phantoms at 10 Hz chopper frequency for 635 nm wavelenght

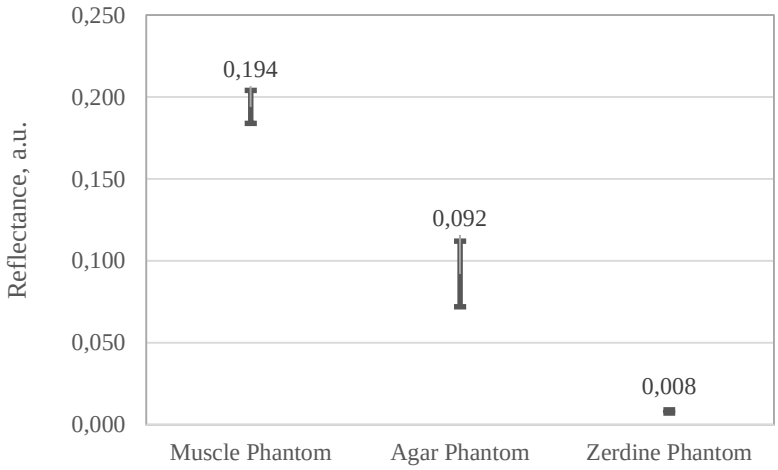

Figure 13. The reflectance values of phantoms at 10 Hz chopper frequency for 635 nm wavelenght

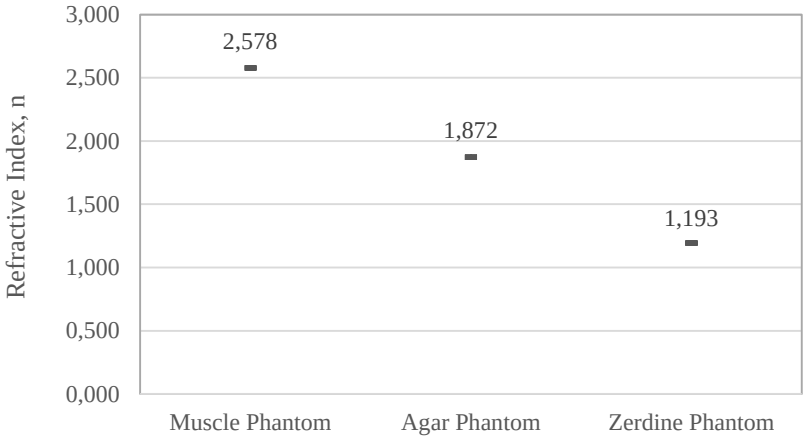

Figure 14. The refractive Index values of phantoms at 10 Hz chopper frequency for 635 nm wavelenght

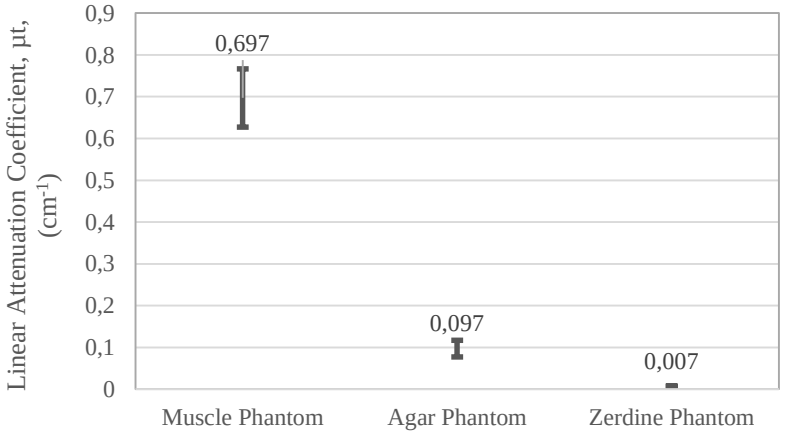

Figure 15. The linear attenuation coefficient values of phantoms at 10 Hz chopper frequency for 635 nm wavelenght

4.3 Calculations of Microscopic Optical Parameters of Phantoms

After determining the macroscopic optical properties, microscopic optical properties such as the absorption coefficient, scattering coefficient, and reduced scattering coefficient at 10 Hz chopper frequency with the help of the Kubelka-Munk function approach were calculated separately for the phantoms at 635 nm wavelength. The calculation results are presented in Figures 16–18.

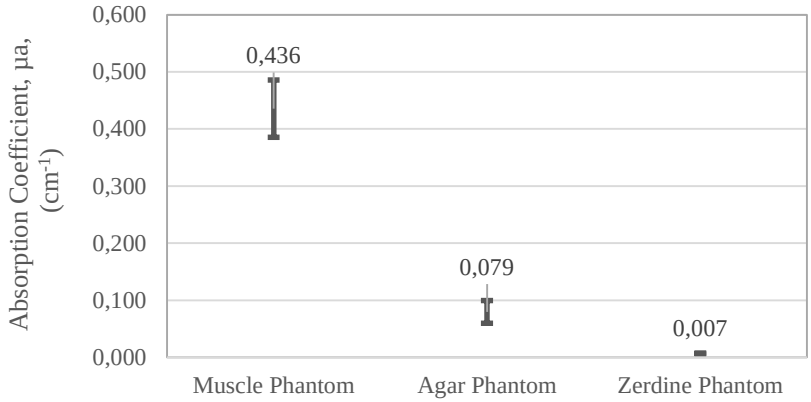

Figure 16. The absorption coefficient values of phantoms at 10 Hz chopper frequency for 635 nm wavelenght

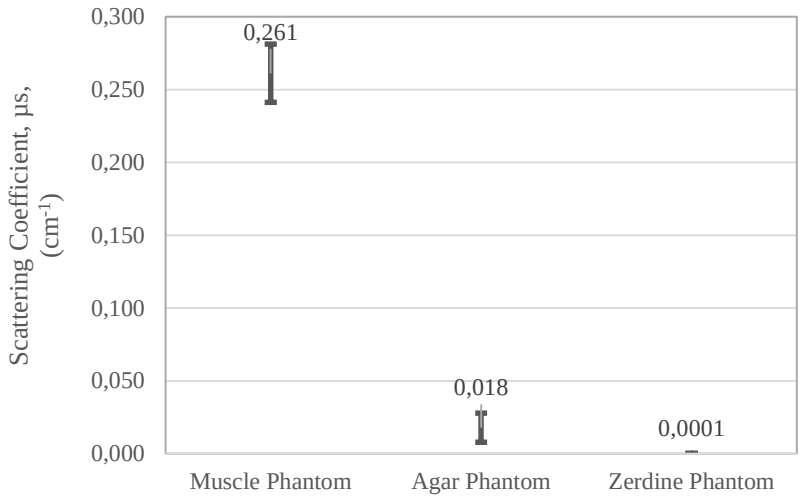

Figure 17. The scattering coefficient values of phantoms at 10 Hz chopper frequency for 635 nm wavelenght

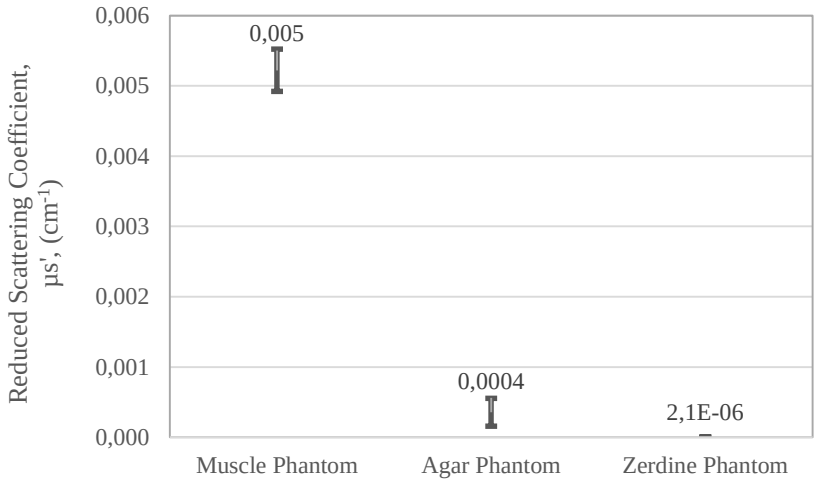

Figure 18. The reduced scattering coefficient values of phantoms at 10 Hz chopper frequency for 635 nm wavelenght

When the correlation of the photoacoustic signal sets of all three phantoms with the density and macroscopic optical parameters was examined, it was found that the absorbance and absorption coefficient were related to 90%. The results are presented in Tables I and II. This shows that the amplitude of the photoacoustic signals depends on the density and macroscopic optical parameters; in other words, it is directly related to the absorption coefficient to a large extent. Therefore, this study confirms the photoacoustic (PA) effect of producing acoustic waves formed by the absorption of modulated electromagnetic waves by materials. The photoacoustic effect is closely related to the absorption capability of chromophores in materials (Bayer, Luke, & Emelianov, 2012).

Furthermore, it also confirms the thesis that photoacoustic imaging can be an imaging method that derives image contrast from the optical absorption coefficient of the imaged tissue (Steinberg, ve diğerleri, 2019) (Zhang, Hong, & Cai, 2011).

Table I. Density and the measured optical parameters

Phantoms	Density	Absorbance	Transmittance	Reflectance	Absorption Coefficient
Muscle	1.07	0.454	0.352	0.194	0.436
Agar	1.06	0.084	0.823	0.092	0.079
Zerdine	0.98	0.006	0.986	0.008	0.007

Table II. Correelation of photoacoustic signal via critical parameters

Parameters	Photoacoustic Signal
Density	0.32
Absorbance	0.89
Transmittance	-0.85
Reflectance	0.72
Absorption Coefficient	0.9

5. CONCLUSION

The results of this study revealed that the established measurement system is a material characterization analyzer that detects photoacoustic effects and produces different electrical signals in different tissue-mimicking materials; it has been proven that photoacoustic effects are directly related to optical parameters such as optical absorbance or absorption coefficient of the material studied. By offering an innovative method, we showed that the macroscopic and microscopic optical parameters of phantoms from photoacoustic measurements can be determined by evaluating the situations when the phantom is in the system and when there is no phantom in the system at a specific chopper frequency. In addition, a measuring "photoacoustic spectroscopy" device can be produced in the future using different color filters together with lock-in signals locked to the chopper frequency. Briefly, this study demonstrated that photoacoustic effects are the basis of photoacoustic technology.

ACKOWLEDGEMENT

We thank our colleagues Assoc. Prof. Dr. Baki Karaböce, Dr. Cengiz Birlikseven and Mithat Özdingiş in the Medical Metrology Laboratory for their technical contributions to the photoacoustic measurement setup.

REFERENCES

Ashton, H. S., MacKenzie, H. A., Rae, P., Shen, Y. C., Spiers, S., & Lindberg, J. (1999). Blood glucose measurements by photoacoustics. *463*(1), s. 570-572.

Baddour, N., & Mandelis, A. (2015). The Effect of Acoustic Impedance on Subsurface Absorber Geometry Reconstruction using 1D Frequency-Domain Photoacoustics. *Photoacoustics, 3*(4), s. 132-142.

Bayer, C. L., Luke, G. P., & Emelianov, S. Y. (2012). Photoacoustic imaging for medical diagnostics. *Acoustics today, 8*(4), 15.

Beard, P. (2011). Biomedical photoacoustic imaging. *Interface focus, 1*(4), 602-631.

Chang, S., & Bowden, A. K. (2019). Review of methods and applications of attenuation coefficient measurements with optical coherence tomography. *Journal of biomedical optics, 24*(9), 090901.

Chen, Q., Qin, W., Qi, W., & Xi, L. (2021). Progress of clinical translation of handheld and semi-handheld photoacoustic imaging. *Photoacoustics, 22*(100264).

Cook, J. R., Bouchard, R. R., & Emelianov, S. Y. (2011). Tissue-mimicking phantoms for photoacoustic and ultrasonic imaging. *Biomedical optics express, 2*(11), s. 3193–3206. doi:10.1364/BOE.2.003193

Culjat, M. O., Goldenberg, D., Tewari, P., & Singh, R. S. (2010). A review of tissue substitutes for ultrasound imaging. *Ultrasound in medicine & biology, 36*(6), s. 861-873.

Gutierrez, M. I., Lopez-Haro, S. A., Vera, A., & Leija, L. (2016). Experimental verification of modeled thermal distribution produced by a piston source in physiotherapy ultrasound. *BioMed research international*.

Haisch, C. (2011). Photoacoustic spectroscopy for analytical measurements. *Meas. Sci. Technol., 23*(012001).

Hariri, A., Lemaster, J., Wang, J., Jeevarathinam, A. S., Chao, D. L., & Jokerst, J. V. (2018). The characterization of an economic and portable LED-based photoacoustic imaging system to facilitate molecular imaging. *Photoacoustics, 9*, 10-20.

Harvey, D. T. (2003). *Analytical Chemistry for Technicians* (3rd Edittion b.). John Kenkel.

Herrmann, K., Pech-May, N., & Retsch, M. (2021). Photoacoustic thermal characterization of low thermal diffusivity thin films. *Photoacoustics, 22*(100246).

Hosseinaee, Z., Le, M., Bell, K., & Reza, P. H. (2020). Towards non-contact photoacoustic imaging [review]. *Photoacoustics, 20*(100207).

Jeong, E. J., Song, H. W., Lee, Y. J., Park, S. J., Yim, M. J., Lee, S. S., & Kim, B. K. (2017). Fabrication and characterization of PVCP human breast tissue-mimicking phantom for photoacoustic imaging. *BioChip Journal, 11*(1), s. 67-75.

Karaböce, B., Çetin, E., Durmuş, H. O., & Özdingiş, M. (2016). Investigation of the temperature effect of ultrasound used in cancer therapy. *In 2016 Medical Technologies National Congress (TIPTEKNO)* (s. 1-4). IEEE.

Keeratirawee, K., & Hauser, P. C. (2021). Photoacoustic detection of ozone with a red laser diode. *Talanta, 223, Part 2*(121890).

Krishnaswamy, S. (2008). *Photoacoustic Characterization of Materials. In Springer Handbook of Experimental Solid Mechanics.* Boston, MA, USA: Springer.

Liu, L., Huan, H., Zhang, X., Zhang, L., Shao, X., & Mandelis, A. (2021). Laser Induced Thermoelastic Contributions from Windows to Signal Background in a Photoacoustic Cell. *Photoacoustics*(100257).

Liu, L., Huan, H., Zhang, X., Zhang, L., Shao, X., Mandelis, A., & Dong, L. (2021). Laser induced thermoelastic contributions from windows to signal background in a photoacoustic cell. *Photoacoustics, 22*(100257).

Manohar, S., & Gambhir, S. (2020). Clinical photoacoustic imaging. *Photoacoustics,, 19*(100196).

McGarry, C. K., Grattan, L. J., Ivory, A. M., Leek, F., Liney, G. P., Liu, Y., & Clark, C. H. (2020). Tissue mimicking materials for imaging and therapy phantoms: a review. *Physics in Medicine & Biology*.

Mehra, N. K., Jain, K., & Jain, N. K. (2016). *Multifunctional carbon nanotubes in cancer therapy and imaging. In Nanobiomaterials in Medical Imaging.* William Andrew Publishing.

Musdal, B. D., & Kurt, M. (2021). Design of EM-artifact-free earphone based on the photoacoustic effect. *Photoacoustics, 21*(100214). doi:10.1016/j.pacs.2020.100214.

Nadeem, M. Y., & & Ahmed, W. (2000). Optical properties of ZnS thin films. *Turkish Journal of Physics, 24*(5), 651-659.

Oraevsky, A., Clingman, B., Zalev, J., Stavros, A., Yang, W., & Parikh, J. (2018). Clinical optoacoustic imaging combined with ultrasound for coregistered functional and anatomical mapping of breast tumors. *Photoacoustics, 12*, 30-45.

Park, S. M., Kim, D. Y., Cho, S.-W., Kim, B.-M., Lee, T. G., Kim, C.-S., & Lee, S.-W. (2020). Quickly Alternating Green and Red Laser Source for Real-time Multispectral Photoacoustic Microscopy. *Photoacoustics, 20*(100204).

PhotoAcoustic Imaging (PAI). (2022). https://www.eurobioimaging.eu/service/photoacoustic-imaging-pai-

Photoacoustic spectroscopy for gas sensing: from theoretical modeling to applications. (2022). https://www.sciencedirect.com/journal/photoacoustics/special-issue/107XM34RKBJ

Pinto, D., Moser, H., Waclawek, J. P., Russo, S. D., Patimisco, P., Spagnolo, V., & Lendl, B. (2021). Parts-per-billion detection of carbon monoxide: A comparison between quartz-enhanced photoacoustic and photothermal spectroscopy. *Photoacoustics, 22*(100244).

Rajeshkumar, G., Vishnupriyan, R., & Selvadeepak, S. (2020). Tissue Mimicking Material an Idealized Tissue Model for Clinical Applications: A Review. *Materials Today: Proceedings*, (s. 2696-2703).

Sawada, T. (1982). *Hikari Onkyou Bunkouhou to Sono Ouyou - PAS [Applications of Photoacoustic Spectroscopy - PAS]*. Japan Scientific Societies Press.

Steinberg, I., Huland, D. M., Vermesh, O., Frostig, H. E., Tummers, W. S., & Gambhir, S. S. (2019). Photoacoustic clinical imaging. *Photoacoustics, 14*, 77-98.

Su, J. L., Wang, B., Wilson, K. E., Bayer, C. L., Chen, Y. S., Kim, S., & Emelianov, S. Y. (2010). Advances in clinical and biomedical applications of photoacoustic imaging. *Expert opinion on medical diagnostics, 4*(6), 497-510.

Subramanian, A. S. (2009). Monitoring flavor quality, composition and ripening changes of Cheddar cheese using Fourier-transform infrared spectroscopy [Doctoral dissertation, The Ohio State University].

Tabaru, T. E., & Saraçoğlu, Ö. G. (2014). Darbeli Lazer Diyot Uyartımlı Fotoakustik Yöntemle Glikoz Algılanması. *Eleco 2014 Elektrik – Elektronik – Bilgisayar ve Biyomedikal Mühendisliği Sempozyumu.* Bursa.

Tan, G. (2018). Photoacoustic analysis and imaging techniques: Sound of light. *Particulate Science and Technology, 36*(1), 29-37. doi:10.1080/02726351.2016.1205689

Thakur, S. N. (2018). Chapter 13 - Photoacoustic Spectroscopy: Applications in Security and Biology. V. Gupta içinde, *Molecular and Laser Spectroscopy* (s. 283-316). Elsevier.

Thouvenot, A., Poepping, T., Peters, T. M., & Chen, E. C. (2016). Characterization of various tissue mimicking materials for medical ultrasound imaging. In Medical Imaging 2016: Physics of Medical Imaging. *International Society for Optics and Photonics, 9783*(97835E).

Torrent, J., & Barrón, V. (2008). Methods of Soil Analysis Part 5—Mineralogical Methods. *Diffuse reflectance spectroscopy.* (s. 367-385).

Volkov, D. S., Rogova, O. B., & Proskurnin, M. A. (2020). Photoacoustic and photothermal methods in spectroscopy and characterization of soils and soil organic matter. *Photoacoustics, 17*(100151).

Wilson, B. C. (1995). In Optical-thermal response of laser-irradiated tissue. *Measurement of tissue optical properties: methods and theories.* (s. 233-303). içinde Boston, MA: Springer.

Zerhouni, M. B., & Rachedine, M. "Ultrasonic calibration material and method," ed: Google Patents. (1993).

Zhang, Y., Hong, H., & Cai, W. (2011). Photoacoustic imaging. *Cold Spring Harbor Protocols*, *9*.

Zhou, J., & Jokerst, J. V. (2020). Photoacoustic imaging with fiber optic technology: A review. *Photoacoustics*, *20*(100211).